Journal of Crystal Growth 595 (2022) 126804

Contents lists available at ScienceDirect

Journal of Crystal Growth

journal homepage: www.elsevier.com/locate/jcrysgro

A Knudsen cell approach for the molecular beam epitaxy of the heavy fermion compound $YbRh_2Si_2$

E. Bakali [a,*], W. Artner [b], M. Beiser [c], J. Bernardi [d], H. Detz [c,e,f], G. Eguchi [a], A. Foelske [g], M. Giparakis [c], C. Herzig [h], A. Limbeck [h], H. Nguyen [a], L. Prochaska [a], A. Prokofiev [a], M. Sauer [g], S. Schwarz [d], W. Schrenk [c,e], G. Strasser [b,e], R. Svagera [a], M. Taupin [a], A.S. Thirsfeld [d], M. Waas [a], X. Yan [a], D.A. Zocco [a], A.M. Andrews [c], S. Paschen [a]

[a] Institute of Solid State Physics, TU Wien, Wiedner Hauptstraße 8-10, 1040 Vienna, Austria
[b] Service Unit of X-ray Centre, TU Wien, Lehargasse 6, 1060 Vienna, Austria
[c] Institute of Solid-State Electronics and Center for Micro- and Nanostructures, TU Wien, Gußhausstraße 25-25a, 1040 Vienna, Austria
[d] Service Unit of University Service Centre for Transmission Electron Microscopy, TU Wien, Wiedner Hauptstraße 8-10, 1040 Vienna, Austria
[e] Department Center for Micro and Nanostructures, TU Wien, Gußhausstraße 25-25a, 1040 Vienna, Austria
[f] Central European Institute of Technology, Brno University of Technology, Purkynova 123, 612 00 Brno, Czech Republic
[g] Analytical Instrumentation Center, TU Wien, Lehargasse 6, 1060 Vienna, Austria
[h] Research Group for Surface Analytics, Trace Analytics and Chemometry, TU Wien, Getreidemarkt 9, 1060 Vienna, Austria

ARTICLE INFO

Communicated by H. Lu

Keywords:
A1. X-ray diffraction
A1. Reflection high energy electron diffraction
A3. Molecular beam epitaxy
B1. Metals
B1. Rare earth compounds
B2. Superconducting materials

ABSTRACT

Thin films of the heavy fermion compound $YbRh_2Si_2$ were grown by molecular beam epitaxy on Ge (001) substrates using effusion cells. As-grown $YbRh_2Si_2$ thin films were characterized by a wide range of characterization techniques. X-ray diffraction yields a set of (00l) peaks, demonstrating epitaxial growth along the crystallographic c direction, with a lattice parameter c ranging from 9.84 Å–9.95 Å. The electrical resistivity shows behavior similar to $YbRh_2Si_2$ films grown previously using electron-beam evaporators for Rh and Si. The most stoichiometric sample appears to have the highest quality: It has the highest intensity ratio of the $YbRh_2Si_2$ (004) diffraction peak to the Ge (004) peak, the highest $R(10\ K)/R(2.3\ K)$ ratio, a smallest surface roughness, and only a small density of surface defects.

1. Introduction

$YbRh_2Si_2$ is an extensively studied material with strong electron correlations, in which the localized f-electron states of Yb hybridize with the conduction electrons, giving rise to strongly renormalized bands, and linear-in-temperature strange metal behavior as the Kondo effect is destroyed at a magnetic-field induced quantum critical point (QCP) [1–5]. In a previous work, thin films of $YbRh_2Si_2$ were grown with electron-beam evaporators for Rh and Si, and with an effusion cell for Yb [4]. The films were characterized by transmission electron microscopy (TEM) and investigated in detail by terahertz time-domain transmission spectroscopy [4]. These experiments revealed singular charge fluctuations at the QCP, thereby providing further evidence for its Kondo destruction nature [4]. Here, we investigate whether an alternative growth technique, with effusion cells for all three elements, is feasible. Because we expected the control of the fluxes to be easier with effusion cells than with electron-beam evaporators, we hoped to obtain films with further optimized quality.

2. Experimental details

$YbRh_2Si_2$ thin films were grown on quarters of 3" Ge (001) wafers (625 μm thick, with a resistivity of ~65 Ω cm) [6] in a RIBER C21 EB 200 molecular beam epitaxy (MBE) system. To remove the native oxide layer, the Ge substrates were kept at 500 °C for two hours in a degas chamber prior to inserting them into the growth chamber. We used a high-temperature (RIBER HT 12) cell for Rh, a medium high-temperature (MHT) cell for Si, and a dual zone low-temperature (DZ-MM) cell for Yb. Yb, Rh, and Si charges were purchased from Ames Laboratory, Kurt J. Lesker, and Azelis, respectively.

Here, we report the growth of five different samples, obtained by varying the growth rate (see Table 1). The aim was to grow stoichiometric epitaxial films in all cases. The Rh and Si cell temperatures were calibrated by growing several elemental films with different thicknesses (determined by spectral reflectance and by ellipsometry for Si) and by fitting the data in Arrhenius plots (Fig. 1(a,b)). For the Yb cell, the

* Corresponding author.
E-mail address: emine.bakali@tuwien.ac.at (E. Bakali).

https://doi.org/10.1016/j.jcrysgro.2022.126804
Received 15 December 2021; Received in revised form 16 May 2022; Accepted 20 July 2022
Available online 28 July 2022

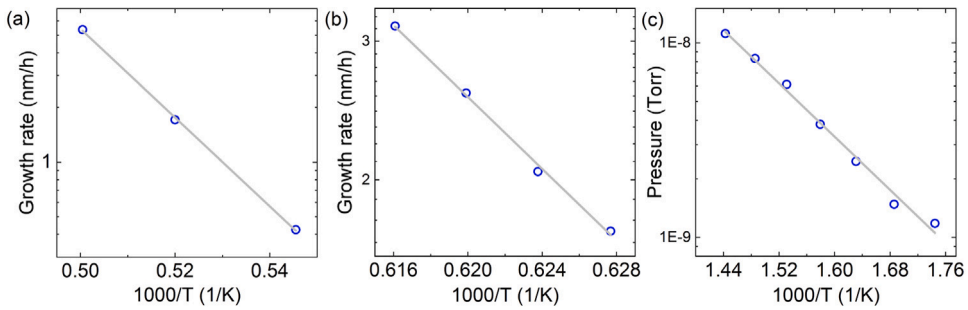

Fig. 1. Arrhenius plots of the growth rates for (a) Rh, (b) Si, and (c) Yb. The gray lines represent linear fits to the data points (blue).

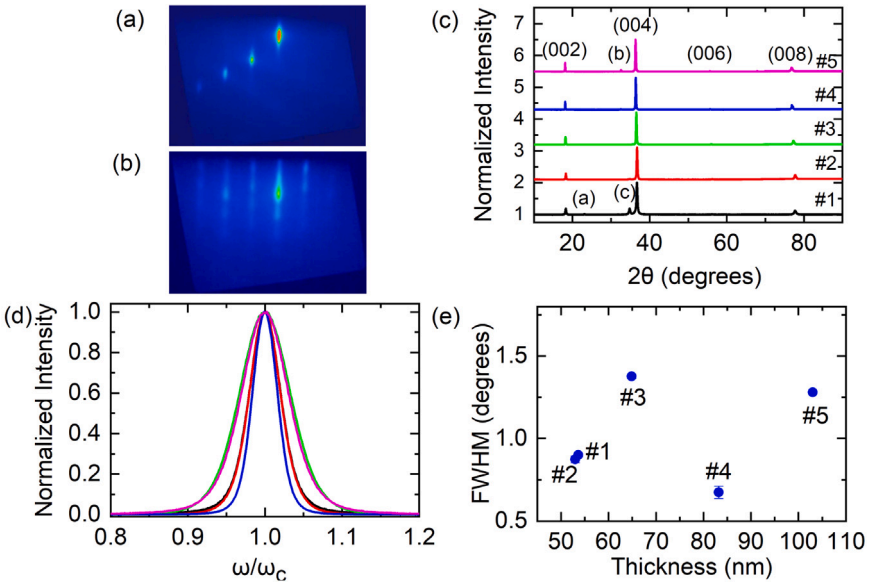

Fig. 2. (a) RHEED pattern of the Ge substrate after oxide removal for film #3. (b) RHEED pattern of the sample #3 after 2 h growth. (c) XRD pattern of five as-grown thin films with the signal from the Ge substrate removed. (d) Rocking curves of the (004) diffraction peak of all five samples (ω_c: center of the peak position), with the same color code as in (c). (e) Mean value of FWHM for the rocking curves of all four $YbRh_2Si_2$ (00l) diffraction peaks vs film thicknesses of the five $YbRh_2Si_2$ thin films. The error bars represent the standard deviation for all four $YbRh_2Si_2$ (00l) diffraction peaks. For most points they are smaller than the symbol size.

Table 1
Growth parameters.

Sample	Growth	Film	Temperature (°C)		
Number	time (hours)	thickness (nm)	Yb base	Rh	Si
#1	22.5		348.6	1609.6	1300.2
#2	15	53.57	354.4	1643.5	1319.5
#3	12	63.07	360.5	1678.6	1339.4
#4	12		363.6	1697.1	1349.7
#5	12		366.8	1715.6	1360.1

calibration was done with a flux gauge (Fig. 1(c)). The growths were all done with the substrate heater at 300 °C, rotating at 10 rpm and under 1.5 $\times 10^{-9}$ torr pressure. For the Si cell, 1360 °C was used as the highest temperature, safely below the melting point of Si. For the Rh cell, the highest temperature was 1715.6 °C.

The structural characterization of the films was done in-situ by reflection high-energy electron diffraction (RHEED) and ex-situ by X-ray diffraction (XRD). The surface morphology of the films was characterized by atomic force microscopy (AFM) and scanning electron microscopy (SEM). Chemical analysis was done by energy-dispersive X-ray spectroscopy (EDX), X-ray photoelectron spectroscopy (XPS), and inductively coupled plasma mass spectroscopy (ICP-MS) after digesting the films with 400 ml diluted acid (3% HNO_3, 1.2% HF, and 3% HCl) in a microwave digestion system at 100 °C. Sample #3 was measured with high-resolution transmission electron microscopy (HR-TEM). The sample preparation for the TEM measurements was done by a focused ion beam (FIB) with Ga ions.

The electrical resistivity was measured using either the van der Pauw or a standard 4-point technique. The films were contacted by wire bonding, using Al wires of 33 μm diameter. Measurements down to 2.3 K were performed in a Quantum Design Physical Property Measurement System (PPMS), and below 2.3 K in dilution refrigerators from Leiden Cryogenics and Oxford Instruments.

3. Results and discussion

The RHEED image of a bare Ge substrate (Fig. 2(a)) shows the typical bulk Ge diffraction spots and Kikuchi lines, which confirms that the oxygen removal was successful. A RHEED image taken after the growth of 5.4 nm of $YbRh_2Si_2$ is shown in Fig. 2(b). It reveals the high degree of (001) orientation of the films. The (0,0) spot is still visible as the brightest spot. The drift in the RHEED spots is due to the substrate rotation during the growth. Fig. 2(c) shows XRD diffraction patterns of five $YbRh_2Si_2$ thin films grown on a Ge (001) substrate. We identified the $YbRh_2Si_2$ (002), (004), (006), and (008) diffraction peaks, confirming the crystallinity of the films. Note that the (006) peak is clearly seen only on a logarithmic scale. The remaining peaks (a, b, c) originate from impurity phases and will be discussed in the next paragraph. To characterize the crystal quality of the $YbRh_2Si_2$ films, rocking curves (RC) of the diffraction peaks were measured. Fig. 2(d)

Table 2
Composition of the $YbRh_2Si_2$ films according to EDX, ICP-MS, and XPS.

	at %, EDX			at %, ICP-MS			at %, XPS		
	Si	Rh	Yb	Si	Rh	Yb	Si	Rh	Yb
# 1	38.5	34.9	26.6	30.4	38.1	31.5			
# 2	38.3	39.6	22.1	32.8	41.7	25.5	40.6	39.6	19.8
# 3	36.0	44.0	20.0	34.2	44.8	21.0	41.7	41.2	17.1
# 4	34.1	51.3	14.6	30.9	52.7	16.4			
# 5	33.0	54.5	12.5	30.4	55.8	13.8			

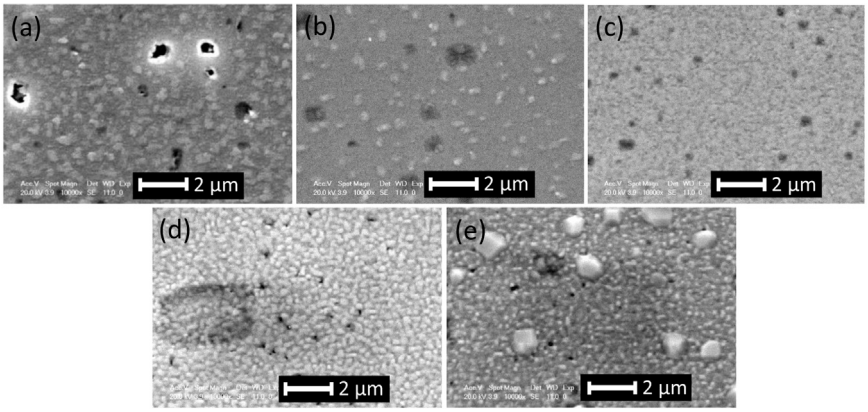

Fig. 3. SEM micrographs of samples #1 to #5 in panels (a) to (e), measured with a secondary electron detector at 10000-fold magnification and with 20 kV energy.

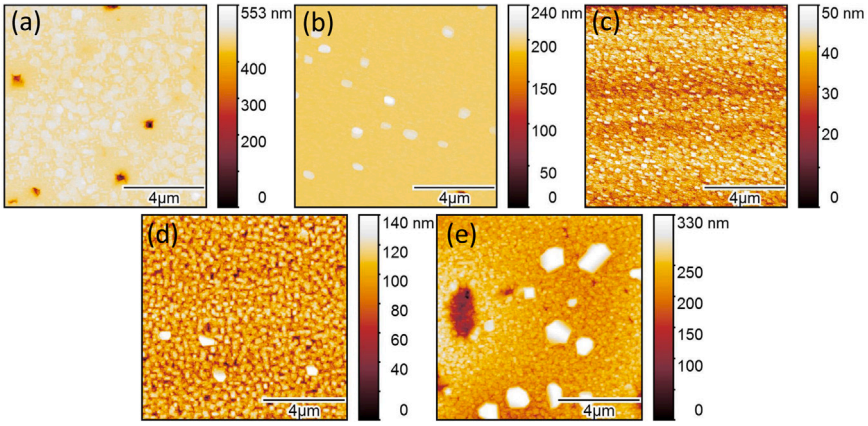

Fig. 4. AFM micrographs of 10 µm × 10 µm areas of samples #1 to #5 in panels (a) to (e). The rms roughnesses are 22.9 nm, 5.33 nm, 10.85 nm, 17.7 nm, and 42.2 nm, respectively.

shows the normalized RC of the (004) diffraction peak of all five films. They are all symmetric. The full width at half maximum (FWHM) was determined for this and the three other diffraction peaks and the mean FWHM value is plotted vs film thicknesses in Fig. 2(e).

The chemical composition of the films as obtained from EDX, ICP-MS, and XPS is summarized in Table 2.

That the Si content from ICP-MS is smaller than that from EDX is due to an experimental artifact: gaseous species were lost during the digestion procedure. With increasing growth rate (from #1 to #5), films evolve from an excess of Yb to an excess of Rh and Si. We will thus be able to use this sample series to further optimize the growth conditions for highly stoichiometric films.

The impurity peaks found in XRD can be identified as the strongest lines of the phases $Yb_{11}Ge_{10}$ and Rh_3Si_2. This is supported by the elemental analysis (Table 2). $Yb_{11}Ge_{10}$ appears in films #1 and #2, which have an excess of Yb. The longer growth times of these two samples might have facilitated a reaction of Yb with the Ge substrate. The formation of Rh_3Si_2 in samples #3, #4, and #5 can be attributed to the excess of Rh and Si in these films. The intensity ratios of the $Yb_{11}Ge_{10}$ diffraction peaks to the $YbRh_2Si_2$ (004) diffraction peaks are 0.140 and 0.005 for samples #1 and #2, respectively. The corresponding ratios for Rh_3Si_2 in samples #3, #4, and #5 are 0.010, 0.027, and 0.048, respectively. To avoid these foreign phases in future growths, a careful adjustment of the three fluxes to the ideal 1:2:2 ratio will be needed, possibly combined with higher growth rates to avoid the reaction of Yb with the substrate.

The surface morphology of the films was characterized by SEM (Fig. 3) and AFM (Fig. 4). All five samples have surface void defects and sample #5 has hillock defects in addition. These surface defects are visible in both the AFM and the SEM images. The surface roughnesses were calculated from a 10 µm × 10 µm area of the AFM images and the density of surface defects was determined from the SEM images. Sample #2 has less surface roughness and less surface defects than the other four samples.

The cross-section of sample #3 was investigated with TEM. Fig. 5(a) focuses on a defect. According to a TEM-EDX map (not shown), the material that penetrates into the Ge substrate is rich in Rh and Si, consistent with the presence of Rh_3Si_2 as determined by XRD. This defect

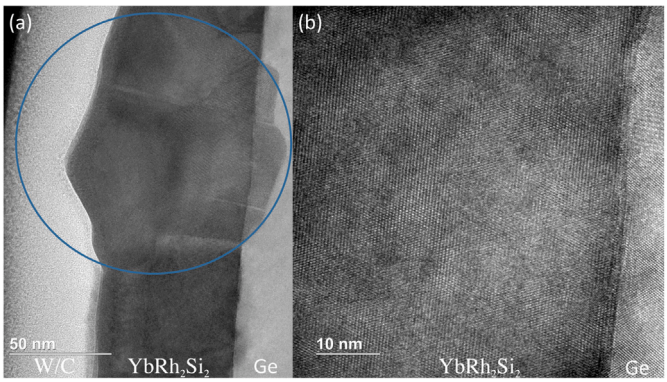

Fig. 5. (a) Cross-section of a TEM scan, at the position of a defect (W/C: tungsten and carbon protection layers for the FIB sample preparation). (b) An HR-TEM image of sample #3, away from the defect.

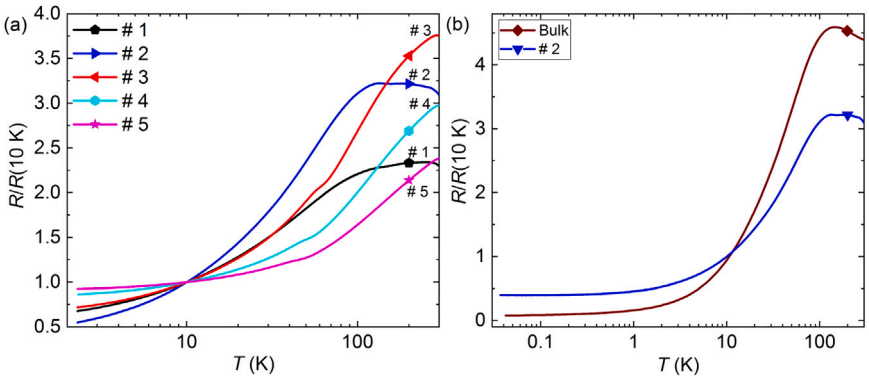

Fig. 6. Temperature-dependent electrical resistances R of the films, normalized to their value at 10 K. (b) Comparison of sample #2 and a bulk single crystal of $YbRh_2Si_2$ [1].

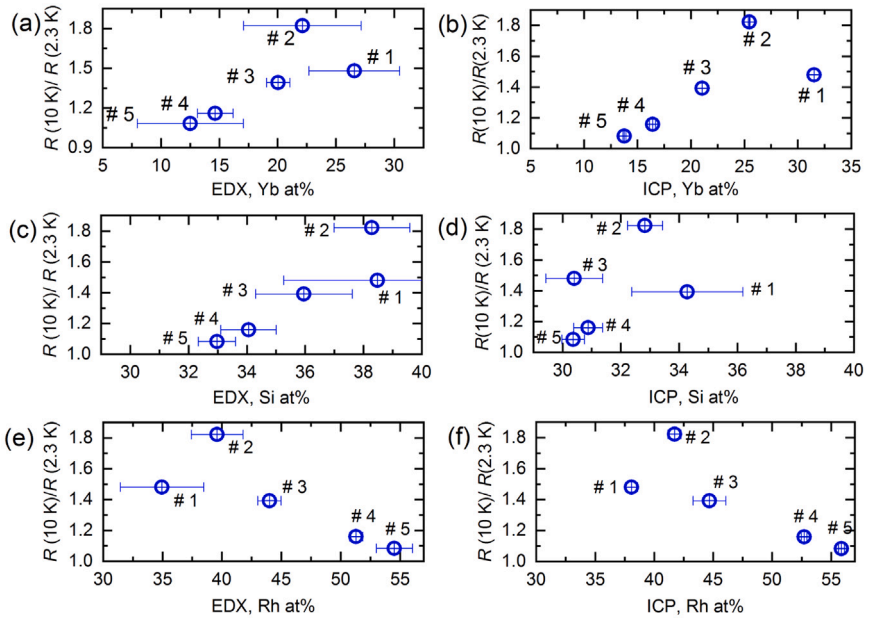

Fig. 7. Evolution of resistance ratio $R(10\,K)/R(2.3\,K)$ with the content of the three elements (Yb, Si, and Rh from top to bottom), determined by EDX (on the left) and ICP-MS (on the right). Note that a loss of Si during the ICP-MS digestion process causes a systematic error in the panels on the right-hand side.

at the beginning of the growth does not seem to heal out as the growth proceeds but extends in form of a different phase throughout the film thickness. Away from such defects, high-resolution TEM (Fig. 5(b)) confirms highly oriented $YbRh_2Si_2$, a rather sharp interface to the Ge substrate, and essentially constant profiles of the three elements across the sample thickness (according to TEM-EDX). To obtain defect-free films, it once again seems essential that the three elements arrive at the substrate in highly stoichiometric ratios.

We now turn to the physical properties. The temperature-dependent electrical resistances of all samples, normalized to their values at

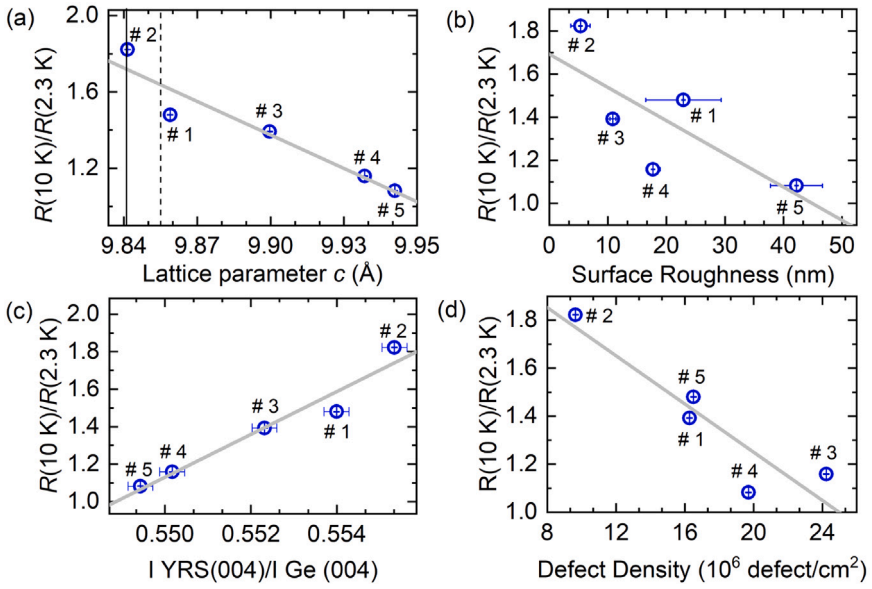

Fig. 8. Evolution of the resistance ratio $R(10\,K)/R(2.3\,K)$ with (a) the lattice parameter c determined by XRD (the solid and dashed vertical lines indicate c of $YbRh_2Si_2$ determined in [1,8], respectively), (b) the surface roughness, (c) the intensity ratio of the (004) diffraction peak of the film to the Ge substrate, and (d) the surface defect density.

10 K ($R/R(10\,K)$), are plotted in Fig. 6(a). The different temperature dependencies are attributed both to deviations from the ideal 1:2:2 stoichiometry in the main phase and to different amounts of impurity phases. To understand the appearance of the double shoulder structure instead of a single maximum as seen in stoichiometric bulk single crystals, we measured the resistance of a bare Ge substrate. Whereas its resistance is orders of magnitude larger than that of the film at low temperatures, and thus plays no role there, it may well have a non-negligible influence at high temperatures. Alternatively, the double shoulder structure might hint at a (negative) pressure effect similar to the (positive) pressure effect observed in [7]. The resistivity ratio $R(10\,K)/R(2.3\,K)$, away from these substrate or pressure effects, is a reliable measure of the film quality. The larger the ratio, the better the quality. Sample #2, which is nearly stoichiometric according to EDX, indeed has the largest $R(10\,K)/R(2.3\,K)$ value (1.82), distinctly larger than the MBE film studied in [4]. Its resistivity trace is similar to that of a bulk single crystal (Fig. 6(b)).

Figs. 7 and 8 display $R(10\,K)/R(2.3\,K)$ as a function of various parameters determined in our study: the atomic percentages of Yb, Rh, and Si, according to EDX (Fig. 7 left) and ICP (Fig. 7 right), the lattice parameter c derived from the XRD 2θ scan (Fig. 8(a)), the surface roughness (Fig. 8(b)), the ratio of the $YbRh_2Si_2$ (004) diffraction peak to the Ge (004) diffraction peak (Fig. 8(c)), and the defect density (Fig. 8(d)). Sample #2, which has the largest $R(10\,K)/R(2.3\,K)$ ratio, is closest to the correct 1:2:2 stoichiometry and the lattice parameter of bulk single crystals (dashed line), has the smallest surface roughness, the largest relative XRD intensity, and the lowest defect density. The overall systematic behavior of all films will help to adjust the growth conditions to further improve the quality of MBE grown $YbRh_2Si_2$.

4. Conclusion

In conclusion, we have succeeded to grow $YbRh_2Si_2$ MBE films utilizing effusion cells for all three elements. The films grow on Ge substrates along the crystallographic c axis. Films that are not stoichiometric contain $Yb_{11}Ge_{10}$ or Rh_3Si_2 precipitation defects. The best film of the present study is the most stoichiometric one. It has the highest $R(10\,K)/R(2.3\,K)$ ratio, higher than that of an MBE film grown previously with electron-beam evaporators for Rh and Si [4], and the lowest surface roughness and defect density. Its resistivity is closest to that of stoichiometric bulk single crystals.

CRediT authorship contribution statement

E. Bakali: Investigation, Writing – original draft. **W. Artner:** Investigation. **M. Beiser:** Investigation. **J. Bernardi:** Investigation, Supervision. **H. Detz:** Investigation. **G. Eguchi:** Investigation, Supervision. **A. Foelske:** Investigation, Supervision. **M. Giparakis:** Investigation. **C. Herzig:** Investigation. **A. Limbeck:** Investigation, Supervision. **H. Nguyen:** Investigation, Supervision. **L. Prochaska:** Investigation. **A. Prokofiev:** Investigation, Supervision. **M. Sauer:** Investigation. **S. Schwarz:** Investigation. **W. Schrenk:** Investigation. **G. Strasser:** Supervision. **R. Svagera:** Investigation. **M. Taupin:** Investigation, Supervision. **A.S. Thirsfeld:** Investigation. **M. Waas:** Investigation. **X. Yan:** Investigation, Supervision. **D.A. Zocco:** Investigation, Supervision. **A.M. Andrews:** Investigation, Supervision. **S. Paschen:** Conceptualization, Investigation, Supervision, Writing – review & editing.

Declaration of competing interest

The authors declare that they have no known competing financial interests or personal relationships that could have appeared to influence the work reported in this paper.

Acknowledgments

This work was supported by the Austrian Science Fund FWF (P29296-N27, P29279-N27, I4047-N27) and by the European Union's Horizon 2020 Research and Innovation Programme, under Grant Agreement no. 824109.

References

[1] O. Trovarelli, C. Geibel, S. Mederle, C. Langhammer, F.M. Grosche, P. Gegenwart, M. Lang, G. Sparn, F. Steglich, $YbRh_2Si_2$: Pronounced non-Fermi-liquid effects above a low-lying magnetic phase transition, Phys. Rev. Lett. 85 (2000) 626–629.

[2] P. Gegenwart, J. Custers, C. Geibel, K. Neumaier, T. Tayama, K. Tenya, O. Trovarelli, F. Steglich, Magnetic-field induced quantum critical point in $YbRh_2Si_2$, Phys. Rev. Lett. 89 (2002) 056402–056405.

[3] S. Paschen, T. Lühmann, S. Wirth, P. Gegenwart, O. Trovarelli, C. Geibel, F. Steglich, P. Coleman, Q. Si, Hall-effect evolution across a heavy-fermion quantum critical point, Nature 432 (2004) 881–885.

[4] L. Prochaska, X. Li, D.C. MacFarland, A.M. Andrews, M. Bonta, E.F. Bianco, S. Yazdi, W. Schrenk, H. Detz, A. Limbeck, Q. Si, E. Ringe, G. Strasser, J. Kono, S. Paschen, Singular charge fluctuations at a magnetic quantum critical point, Science 367 (2020) 285–288.

[5] D.H. Nguyen, A. Sidorenko, M. Taupin, G. Knebel, G. Lapertot, E. Schuberth, S. Paschen, Superconductivity in an extreme strange metal, Nat. Commun. 12 (2021) 4341.
[6] Ge wafers (001), Ingot number: n099 1011-2, 2016, https://www.umicore.com.
[7] G. Dionicio, H. Wilhelm, G. Sparn, J. Ferstl, C. Geibel, F. Steglich, Electrical resistivity of $YbRh_2Si_2$ at high pressure, Physica B 359–361 (2005) 50–52.
[8] D. Rossi, R. Marazza, R. Ferro, Ternary RME_2x_2 alloys of the rare earths with the precious metals and silicon (or germanium), J. Less-Common Met. 66 (1979) P17–P25.